

Evanescent wave spectral singularities in non-Hermitian photonics

Huan He^{1,*}, Zhaoxian Chen^{2,*}, Huanan Li^{1,†}, Cheng-Hou Tu,¹ Jingjun Xu,^{1,‡} and Andrea Alù^{3,4,§}

¹MOE Key Laboratory of Weak-Light Nonlinear Photonics, School of Physics, Nankai University, Tianjin 300071, China

²College of Engineering and Applied Sciences, Collaborative Innovation Center of Advanced Microstructures, and National Laboratory of Solid State Microstructures, Nanjing University, Nanjing 210023, China

³Photonics Initiative, Advanced Science Research Center, City University of New York, New York, New York 10031, USA

⁴Physics Program, Graduate Center, City University of New York, New York, New York 10016, USA



(Received 7 July 2023; revised 13 November 2023; accepted 17 December 2023; published 16 January 2024)

Spectral singularities (SSs) emerge at isolated real frequencies when the scattering coefficients of a system diverge, producing scattering anomalies in non-Hermitian systems. Here, based on parity-time symmetry, we introduce SSs for evanescent waves, and explore their exotic features. We show that evanescent wave SSs can realize highly reconfigurable unidirectional lasers and absorbers, and offer the opportunity to observe extreme scattering anomalies associated with SSs in fully passive platforms, decoupling their extreme scattering responses from energy considerations. More broadly, our study opens avenues for non-Hermitian wave engineering, showcasing a link between non-Hermitian physics and structured waves, with implications in nano-optics for extreme wave-matter interactions and functional devices.

DOI: [10.1103/PhysRevB.109.L041405](https://doi.org/10.1103/PhysRevB.109.L041405)

Introduction. Structured waves with inhomogeneous wavefields underpin modern optics and photonics, crucial in various technical areas of physics, such as microscopy, imaging, and communications [1]. Arguably, the most common form of structured waves are evanescent plane waves, i.e., oscillating fields with amplitude modulation due to an imaginary wavevector component. They play an important role in photonic systems, from conventional near-field interactions, to more exotic responses, such as super-Planckian thermal emission [2–9] and subdiffraction imaging [10,11]. Evanescent wave engineering can also be used to modify the local boundary conditions at an interface, enabling extreme asymmetry in metasurfaces [12,13], enhanced propagation through opaque media [14], and the formation of exotic frozen mode regimes for slow light [15–19]. Recently, the complex-field nature of evanescent waves was used to realize a gain-free platform for parity-time (*PT*) symmetry in photonics [20], enabling features typical of *PT*-symmetric systems, such as phase transitions and anisotropic transmission resonances (ATRs) [21].

Non-Hermitian physics has unveiled a new paradigm for wave engineering by utilizing tailored spatial distributions of gain and loss [22–28]. In non-Hermitian photonic systems, spectral singularities (SSs) can emerge, associated with diverging scattering coefficients at real frequencies [29]. In optics, SSs correspond to lasing at threshold [30] and, when combined with *PT* symmetry, can yield laser-absorber pairs [31,32]. By incorporating Fano resonances, a laser-absorber pair can support unidirectional SSs, enabling simultaneously

infinite and zero reflection coefficients when excited from opposite sides [33], of great interest for directional wave-matter interactions.

So far, the emergence of these exotic SSs has been restricted to propagating waves [34–40]. Here, we extend them to evanescent waves and show that, due to the decoupling between energy transport and scattering strength for evanescent waves, an evanescent wave SS with diverging scattering coefficients can support arbitrary magnitude (infinite or finite) and reversible energy flow, depending on how the evanescent wave SS is approached in parameter space. To this end, we construct a non-Hermitian framework to implement both unidirectional and ordinary SSs for evanescent waves, providing a strategy for unidirectional lasing and absorption, and enabling extreme scattering responses even in purely passive settings.

Evanescent waves in coupled-resonator optical waveguides. Evanescent wave propagation is ubiquitous in photonics. As a canonical platform, we consider a coupled-resonator optical waveguide (CROW), consisting of an array of coupled resonators with individual eigenfrequency u_c , coupling strength κ_c , and periodicity a [41], with dispersion $\omega = u_c - 2\kappa_c \cos qa$. For convenience, we choose a frequency reference by setting $u_c = 0$, and adopt a natural unit system assuming $\kappa_c = a = 1$. For excitation frequency $\omega > 2$ (or $\omega < -2$), the wave number q with $\text{Re}(q) = \pi$ (or 0) picks up a nonzero imaginary part, and evanescent waves emerge [42]. Their time-dependent energy-normalized complex amplitude $\psi(n, t)$ in steady state reads

$$\psi(n, t) = F e^{j\omega t - jqn} + B e^{j\omega t + jqn}, \quad (1)$$

where the integer n labels CROW sites, and $\sin q = \mp \sqrt{\omega^2 - 4}/(2j)$ when $\omega > 2$ ($\omega < -2$), involving forward (backward) evanescent waves of amplitude F (B) decaying

*These authors contributed equally to this work.

†hli01@nankai.edu.cn

‡jjxu@nankai.edu.cn

§aalu@gc.cuny.edu

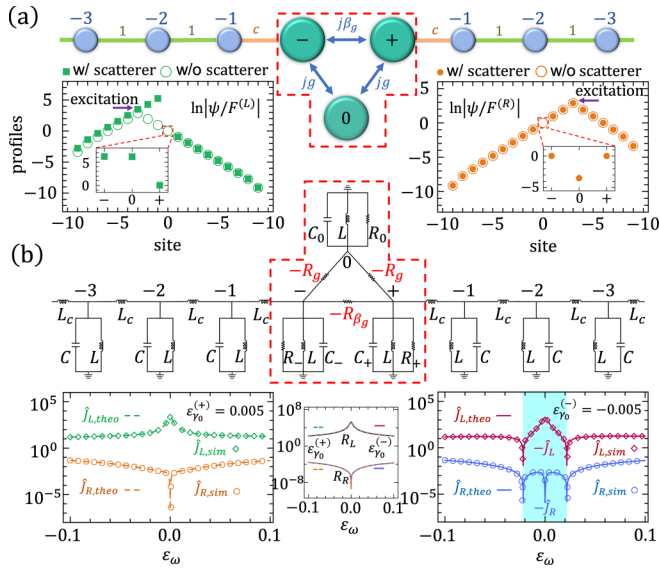


FIG. 1. (a) Upper panel: schematic of the geometry formed by a three-site defect (dashed red box) embedded in a CROW. Lower panels: logarithm of the (normalized) field profiles $|\psi/F^{(\alpha)}|$ in the scattering setup with (without) the scatterer for evanescent wave excitation at $\omega = \omega_0$ from left ($\alpha = L$) (left panel) and right ($\alpha = R$) (right panel), respectively, near the evanescent wave unidirectional SS with detuning $\varepsilon_{\gamma_0} = \varepsilon_{\gamma_0}^{(+)} = 0.005$ of the conditions $s^{(uSS)}$. The locations of the excitation sources are indicated by purple arrows, and the insets depict the scatterer-related field profiles at sites $-$, 0 , and $+$. (b) Upper panel: one circuit analog of the theoretical model in (a). Lower panels: normalized energy flux \hat{J}_α at the excitation port $\alpha = L, R$ versus the frequency detuning ε_ω when ε_{γ_0} switches from $\varepsilon_{\gamma_0}^{(+)}$ (left panel) to $\varepsilon_{\gamma_0}^{(-)} = -0.005$ (right panel), with the associated left (right) reflectance $R_{L(R)}$ in the middle panel. The colored background in the right panel highlights the negative sign of \hat{J}_α , and the results of the theoretical model (lines) match well with those of circuit simulations (symbols) [44]. Other free parameters are $g = \gamma = 0.1$, $c = 1$, and $\omega_0 = 3$.

towards the sites of larger (smaller) n . Associated with Eq. (1), the energy flux from site n to $n + 1$ is [16,18,20]

$$J_{n \rightarrow n+1} = 4j \sin q \operatorname{Im}(FB^*), \quad (2)$$

independent of position n , where $*$ represents complex conjugation. In contrast with propagating waves, a single evanescent wave *does not* carry energy [11], and the energy flux $J_{n \rightarrow n+1}$ in Eq. (2) is nonzero only when two evanescent waves decay in opposite directions and interfere, i.e., F and B in Eq. (1) are simultaneously nonzero (see also Ref. [43]).

PT-symmetric scattering for evanescent waves. When encountering a defect in the direction of decay, an evanescent wave experiences scattering, like propagating waves. Consider the setup shown in Fig. 1(a), where a scatterer composed of three coupled resonators is embedded in the CROW. The left and right uniform sections of the CROW constitute two ports, and the coupling strengths between the two ports and the scatterer are c . To implement a *PT*-symmetric response for evanescent waves [20], we engineer the effective Hamiltonian H_{eff} for wave evolution within the three coupled resonators

($n = 0, \mp$) as

$$H_{\text{eff}} = \begin{bmatrix} \omega_- + j\gamma_- & jg & j\beta_g \\ jg & \omega_0 + j\gamma_0 & jg \\ j\beta_g & jg & \omega_+ + j\gamma_+ \end{bmatrix}, \quad (3)$$

where the diagonal terms are complex resonant frequencies with real parts $\{\omega_0, \omega_\mp\}$ denoting resonance frequencies and imaginary parts $\{\gamma_0 > 0, \gamma_\mp = \gamma > 0\}$ capturing the damping, while the off-diagonal elements $jg, j\beta_g$ represent the imaginary couplings [Fig. 1(a)]. Due to the assumed imaginary couplings, the scatterer described by H_{eff} is passive when passivity constraint conditions (PCCs) hold, i.e., $\gamma \geq \beta_g \geq 2g^2/\gamma_0 - \gamma$ [44]. We also assume $\omega_0 = \omega_{\text{avg}}/(1 - c^2/2) > 2$, where $\omega_{\text{avg}} \equiv (\omega_+ + \omega_-)/2$. The corresponding setup in Fig. 1(a) supports Fano resonances due to the coupling of the localized state in resonator $n = 0$ with the resonator chain states [33,47].

Different from Ref. [20] using an anti-*PT*-symmetric scatterer, the Hamiltonian H_{eff} in Eq. (3) when $\omega_0 \neq \omega_{\text{avg}}$ does not anticommute with a joint *PT* operation [48]. Nevertheless, the engineered non-Hermitian configuration in Fig. 1(a) can enable a *PT*-symmetric response for evanescent wave excitations. To show this, we label the sites in the left and right CROW ports symmetrically, and calculate the generalized scattering matrix $S(\omega)$ [49] defined via $\begin{pmatrix} B^{(L)} \\ B^{(R)} \end{pmatrix} = S(\omega) \begin{pmatrix} F^{(L)} \\ F^{(R)} \end{pmatrix} \equiv \begin{pmatrix} r_L & t_{LR} \\ t_{RL} & r_R \end{pmatrix} \begin{pmatrix} F^{(L)} \\ F^{(R)} \end{pmatrix}$, which relates the amplitudes $B^{(\alpha)}$ and $F^{(\alpha)}$ of the backward and forward evanescent waves in the left ($\alpha = L$) and right ($\alpha = R$) CROW ports [see Eq. (1)]. By setting the excitation frequency $\omega > 2$, and thus operating in the band gap, the explicit form of $S(\omega)$ reads [44]

$$S(\omega) = -I_2 + 2jc_r(\omega)M[H_{ev}(\omega) + jc_r(\omega)M^T M]^{-1}M^T, \quad (4)$$

where $c_r(\omega) \equiv c^2\sqrt{\omega^2 - 4}/2$, I_N is the $N \times N$ identity matrix, the matrix $M \equiv \begin{bmatrix} 1 & 0 & 0 \\ 0 & 0 & 1 \end{bmatrix}$ (and its transpose M^T) describes the connectivity between ports and scatterer, and the effective Hamiltonian of the scatterer becomes $H_{ev}(\omega) = H^{(PT)} + j(\omega - \omega_0)(I_3 - M^T M c^2/2)$ with

$$H^{(PT)} = \begin{bmatrix} \gamma + j\Delta\omega & g & \beta_g \\ g & \gamma_0 & g \\ \beta_g & g & \gamma - j\Delta\omega \end{bmatrix}, \quad \Delta\omega \equiv \frac{\omega_+ - \omega_-}{2}. \quad (5)$$

This transformation implies that the response of a scatterer is attributed to both the system and the impinging wave. It follows the transformation in Ref. [50] to induce *PT* symmetry in the absence of gain using a transient response, but now for operation in *stationary* states. Indeed, the effective Hamiltonian $H_{ev}(\omega_0) = H^{(PT)}$ ensures that the scattering response of evanescent wave excitations at *real-valued* $\omega = \omega_0$ is *PT* symmetric, since the commutator $[H^{(PT)}, PT] = 0$, with parity operator P exchanging resonators $n = \mp$ and time-reversal operator T performing complex conjugation. Consequently, $S(\omega)$ in Eq. (4) satisfies the fundamental relation $PT S(\omega_0) PT = S(\omega_0)^{-1}$ describing *PT*-symmetric scattering in the stationary state [32], and the

effective gain and loss parameters $\Delta\omega$ are determined by the frequency detuning between resonators $n = \pm$ [Eq. (5)].

Unidirectional SSs for evanescent waves. Following from the PT symmetry of $S(\omega_0)$ in Eq. (4) and the reciprocity $t_{LR} = t_{RL} \equiv t_S$ [51], the scattering coefficients of the structure in Fig. 1(a) satisfy the pseudo-unitary conservation (PUC) relation $\sqrt{R_L R_R} = |T_S - 1|$ at ω_0 for evanescent wave excitations, where the left (right) reflectance $R_{L(R)} \equiv |r_{L(R)}|^2$ and the transmittance $T_S \equiv |t_S|^2$. Unlike propagating waves, the reflectances $R_{L(R)}$ and transmittance T_S for evanescent waves do not correspond to power ratios, due to the inherent absence of energy transport in individual evanescent waves. Notably, the squared amplitudes $|F|^2$ ($|B|^2$) of forward (backward) evanescent waves do not correspond to the power $J_{n \rightarrow n+1} \propto \text{Im}(FB^*)$, as described in Eqs. (1) and (2). Nevertheless, the metrics $R_{L(R)}$ and T_S , derived from the squared amplitudes here, are intrinsically linked to the scattering strength of evanescent wave excitation upon encountering a scatterer. This connection enables us to introduce the concept of evanescent wave SSs when $R_{L(R)}$ and/or T_S diverge, resembling the behavior of SSs observed in propagating waves.

The PUC relationship supports an exotic unidirectional SS [33], when the *finite-valued* transmittance $T_S \neq 1$ and thus one reflectance $R_{R(L)} \rightarrow 0$ implies that the other reflectance $R_{L(R)} \rightarrow \infty$, or vice versa. This phenomenon is dramatically different from that of ATR in PT -symmetric systems for which one between finite R_L and R_R vanishes, and thus $T_S = 1$ [21]. We confirm this finding in the setup of Fig. 1(a): to facilitate searching for a unidirectional SS, we employ the *decimation* procedure [52], initially introduced in the renormalization techniques for statistical mechanics [53], to reduce the dimension of the effective Hamiltonian H_{eff} in Eq. (3) of the scatterer without altering its physical properties. Accordingly, the generalized $S(\omega)$ matrix for evanescent waves [see Eq. (4)] reads [44]

$$S(\omega) = -I_2 + 2jc_r(\omega)[\tilde{H}_{ev}(\omega) + jc_r(\omega)I_2]^{-1}, \quad (6)$$

Involving the reduced 2×2 Hamiltonian $\tilde{H}_{ev}(\omega) = \tilde{H}^{(PT)}(\omega) + j\varepsilon_\omega(1 - c^2/2)I_2$, equivalent to the 3×3 effective Hamiltonian $H_{ev}(\omega)$, but in which the renewed PT -symmetric part $\tilde{H}^{(PT)}(\omega) = \begin{bmatrix} \tilde{\gamma}(\omega) + j\Delta\omega & \tilde{\beta}_g(\omega) \\ \tilde{\beta}_g(\omega) & \tilde{\gamma}(\omega) - j\Delta\omega \end{bmatrix}$ [with renormalized parameters $\tilde{\beta}_g(\omega) = \beta_g + jg^2/(\varepsilon_\omega - j\gamma_0)$ and $\tilde{\gamma}(\omega) = \gamma + jg^2/(\varepsilon_\omega - j\gamma_0)$], and the frequency detuning $\varepsilon_\omega \equiv \omega - \omega_0$.

For PT -symmetric scattering at $\omega = \omega_0$, i.e., $\varepsilon_\omega = 0$, a specific nonunitary transmittance $T_S = 0$ is obtained when $\beta_g = g^2/\gamma_0$, and thus the renormalized coupling $\tilde{\beta}_g(\omega_0) = 0$, corresponding to decoupled resonators at $n = \mp$, and enabled by the Fano resonances. In this case, the right reflectance $R_R \propto (\Delta\omega + c_r(\omega_0))^2 + (\beta_g - \gamma)^2$ vanishes when $\beta_g = \gamma$ and $\Delta\omega = -c_r(\omega_0)$, simultaneously leading to infinite left reflectance, i.e., $R_L \rightarrow \infty$, due to the PUC relation at PT symmetry. Hence, we find an evanescent wave unidirectional SS at ω_0 , supported under the conditions $s^{(uSS)} = \{\beta_g = \gamma, \gamma_0 = g^2/\gamma, \Delta\omega = -c_r(\omega_0)\}$. We can verify this unidirectional SS by studying the frequency response around ω_0 . Specifically, we impose the conditions $s^{(uSS)}$, and examine the behavior of the scattering coefficients as the frequency

detuning $\varepsilon_\omega \rightarrow 0$. By employing Eq. (6), we find that the right reflection $r_R \propto \varepsilon_\omega \rightarrow 0$, while the left reflection $r_L \propto 1/\varepsilon_\omega \rightarrow \infty$, and the finite transmission amplitude limit $t_S = \gamma^2/[(c^2/2 - 1 - c'_r(\omega_0))g^2 - \gamma^2]$. Therefore, the defining features of a unidirectional SS for evanescent waves are exhibited as $\omega \rightarrow \omega_0$, although, due to the absence of precise PT symmetry away from ω_0 [54], the limiting values of the scattering coefficients $r_{R(L)}$ and t_S do not obey the PUC relation.

Properties of evanescent wave SSs. In contrast to SSs for propagating waves [29], evanescent wave SSs exhibit intriguing features, in particular, in the context of energy flow [see Eq. (2)]. For excitation from one port, the transmitted evanescent wave does not carry energy, while the infinite reflection at the SS enables energy flow of arbitrary magnitude (infinite or finite) and reversible direction, depending on the varying interaction between incident and the reflected evanescent waves as the system approaches the SS from different paths in parameter space. At a unidirectional SS driven by PT symmetry, the zero reflection for excitation from the opposite port ensures complete suppression of energy flow, so that the scatterer cannot be detected from one side, while yielding large reflections from the other side, with intriguing applications for sensing.

To demonstrate these features, we first vary the damping coefficient γ_0 of resonator $n = 0$ around the conditions $s^{(uSS)}$, so that $\gamma_0 = g^2/\gamma + \varepsilon_{\gamma_0}$. Interestingly, the right reflection $r_R(\omega_0) \equiv 0$ in this case, leads to the unitary transmittance ($T_S = 1$) based on the PUC relation, while the left reflection $r_L(\omega_0) = [2jc_r(\omega_0)/\gamma][1 + g^2/(\gamma\varepsilon_{\gamma_0})]$ approaches infinity as $\varepsilon_{\gamma_0} \rightarrow 0$ due to the approached unidirectional SS. The corresponding normalized field profile, $\ln|\psi/F^{(\alpha)}|$, in the stationary state for left ($\alpha = L$) [and right ($\alpha = R$)] excitation of the scatterer, is shown in the lower left (and right) panel of Fig. 1(a), where a small detuning $\varepsilon_{\gamma_0} = 0.005$ was assumed, plus free parameters $\gamma = g = 0.1$, $c = 1$, and $\omega_0 = 3$. The excitation source is positioned at the site $n = -3$ (purple arrow) in either the left or the right port. Without a scatterer, evanescent waves decay exponentially in both directions from the source (empty circles). Introducing the scatterer with unidirectional SS, left and right impinging evanescent waves experience dramatically different scattering phenomena. Under left incidence, the total field (filled symbols) grows towards the scatterer due to large reflection (lower left panel), while right incidence results in alignment with the incident wave (lower right panel) since $r_R(\omega_0) = 0$. In both cases, transmitted evanescent waves remain unchanged due to unitary transmittance, and scatterer-related field profiles at the sites $n = -, 0, +$ are exhibited in insets.

If the detuning ε_{γ_0} switches sign, the large left reflectance R_L and small right reflectance R_R are not affected [Fig. 1(b), lower middle panel]. Remarkably, however, the (normalized) energy flux $\hat{J}_\alpha \equiv J_{n \rightarrow n+1}^{(\alpha)}/|F^{(\alpha)}|^2 = 2\sqrt{\omega^2 - 4} \text{Im}(r_\alpha)$ [using Eq. (2)] flowing at the excitation port $\alpha = L, R$ swaps sign near frequency $\omega = \omega_0$ [Fig. 1(b), lower left and right panels], so that the direction of the energy flow is reversed and the operation switches from a unidirectional absorber [$\hat{J}_L(\omega_0) \rightarrow +\infty$, as $\varepsilon_{\gamma_0} \rightarrow 0^+$] to a unidirectional laser [$\hat{J}_L(\omega_0) \rightarrow -\infty$, as $\varepsilon_{\gamma_0} \rightarrow 0^-$]. The performance of the unidirectional absorber and laser here is ideal, in the sense that, in addition to zero-energy leakage at the opposite port, neither unwanted

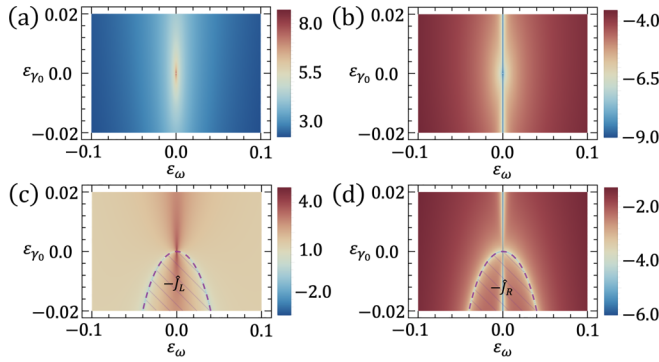


FIG. 2. Density plot of the base-10 logarithm of the reflectance (a) R_L [(b) R_R] and the (normalized) energy flux magnitude (c) $|\hat{J}_L|$ [(d) $|\hat{J}_R|$] at the excitation port versus the detuning $(\varepsilon_\omega, \varepsilon_{\gamma_0})$ of the unidirectional SS, in the case for left (right) impinging evanescent waves. The shaded portions in (c) and (d) differentiate the *negative* energy fluxes from the positive ones of the rest. Other parameters are the same as in Fig. 1.

energy absorption nor emission emerge [i.e., $\hat{J}_R(\omega_0) = 0$], nor is the scatterer detected from the unwanted port [i.e., $r_R(\omega_0) = 0$]. Our predictions are verified by realistic circuit simulations using COMSOL MULTIPHYSICS (see the symbols in Fig. 1), where the sites in the upper panel of Fig. 1(a) are modeled with RLC resonators and the real and imaginary couplings are implemented via series inductors L_c and negative resistors $-R_{g,\beta_g}$, respectively [see Fig. 1(b), upper panel and [44]].

The above features persist as ε_{γ_0} grows [see Fig. 2 for density plots (with saturated color bars at extreme values) of the reflectance (a) R_L and associated energy flux (c) \hat{J}_L on a base-10 logarithmic scale for left excitation, and of (b) R_R and (d) \hat{J}_R for right excitation]. The flux $\hat{J}_\alpha < 0$, $\alpha = L, R$ in the shaded areas of Figs. 2(c) and 2(d), whose boundaries are given by $\varepsilon_\omega^2 = -\varepsilon_{\gamma_0}(\varepsilon_{\gamma_0} + g^2/\gamma)$ and determined from $\hat{J}_\alpha = 0$. The power output is enabled since the scatterer becomes active when the detuning $\varepsilon_{\gamma_0} < 0$ [and thus H_{eff} in Eq. (3) violates PCCs]. In the circuit analog [Fig. 1(b), upper panel], this transition is emulated by increasing the resistance R_0 (inversely correlated with γ_0) above a threshold value so that the ports can draw energy from the fixed negative coupling resistors. We can expect that, once crossing the SS by changing the sign of ε_{γ_0} and thus working past the lasing threshold, the response will be taken over by nonlinear dynamics [56,57].

Next, we explore the response as we vary the effective gain and loss parameter $\Delta\omega$ [Eq. (5)] around the same evanescent wave SS as before so that $\Delta\omega = -c_r(\omega_0) + \varepsilon_{\Delta\omega}$. Different from the previous scenario, this scheme, dictated by H_{eff} in Eq. (3) adhering to PCCs, can be supported within a fully passive setting. In Fig. 3, we show the density plots as in Fig. 2 but against $\varepsilon_{\Delta\omega}$ and the frequency detuning ε_ω . As $\varepsilon_{\Delta\omega} \rightarrow 0$, the left [$R_L(\omega_0) \rightarrow \infty$] and right [$R_R(\omega_0) \rightarrow 0$] reflectances are dramatically different [Figs. 3(a) and 3(b)], yet the energy flux $\hat{J}_\alpha(\omega_0)$ vanishes identically for both the left ($\alpha = L$) and the right ($\alpha = R$) excitations [Figs. 3(c) and 3(d)]. For each excitation frequency $\omega \neq \omega_0$, the local minima

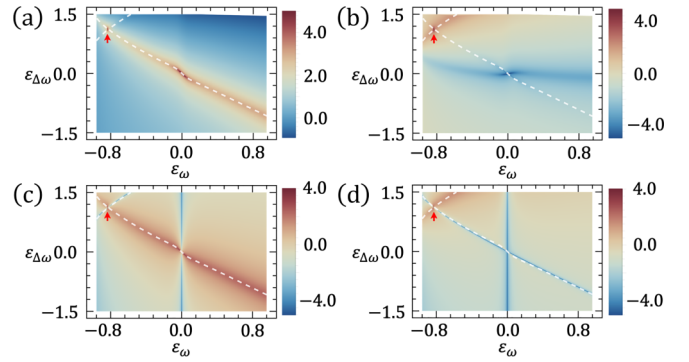


FIG. 3. Density plot of the logarithm of the reflectances (a),(b) $R_{L,R}$ and the energy fluxes (c),(d) $\hat{J}_{L,R} > 0$ (see Fig. 2), versus the detuning $(\varepsilon_\omega, \varepsilon_{\Delta\omega})$ of the evanescent wave unidirectional SS. The white dashed lines trace the trajectories of the local minima of $|Q|$ regarding $\varepsilon_{\Delta\omega}$, and the red arrow indicates their crossing point where $Q = 0$. Other parameters are the same as in Fig. 2.

of the magnitude of $Q \equiv \det[\tilde{H}_{ev}(\omega) + jc_r(\omega)I_2]$ [see Eq. (6)] follow the white dashed lines in Fig. 3. An ordinary SS for evanescent waves is found at $(\varepsilon_\omega, \varepsilon_{\Delta\omega}) = (-5/6, \sqrt{5}/2)$ (red arrow), where two white dashed lines cross, and $Q = 0$, associated with a real-frequency pole of the S matrix in Eq. (6) [58]. At the ordinary SS, both reflectances $R_{L(R)}$ and transmittance T_S (not shown) become infinite, like those occurring at conventional SS for propagating waves but now associated with surface wave resonances (see Refs. [59,60]), with vanishing spectral width. Thanks to the intriguing decoupling of the energy fluxes $\hat{J}_\alpha \propto \text{Im}(r_\alpha)$ [Figs. 3(c) and 3(d)] from the reflectances $R_\alpha = |r_\alpha|^2$ [Figs. 3(a) and 3(b)], however, this scheme enables observing SSs in a fully passive platform, somewhat consistent with [61–63].

Conclusions. In this Letter, we extended the concept of SSs to evanescent waves and explored their unique features in terms of energy flow. By generalizing gain-free PT symmetry for evanescent waves to a regime in which gain and loss may occur, we have constructed a non-Hermitian model supporting both unidirectional SSs with suppressed reflection from one side and ordinary SSs without directionality. Depending on how we approach the SS in parameter space, the infinite reflection at the SS can induce infinite outgoing (incoming) and zero-energy flow with extreme tunability, providing a strategy for flexible unidirectional lasing and absorption, and also enabling the observation of SSs in passive (and thus inherently stable) physical platforms. We have verified our concept in full-wave circuit simulations, shedding light on the opportunity to manipulate structured waves for extreme wave-matter interactions based on non-Hermitian physics, which may be extended to nanophotonics and acoustics [64].

Acknowledgments. This work was supported by the National Natural Science Foundation of China (Grants No. 12274240 and No. 92250302), the Air Force Office of Scientific Research, the Simons Foundation, and the Fundamental Research Funds for the Central Universities (Grant No. 010-63233003).

- [1] K. Y. Bliokh, E. Karimi, M. J. Padgett, M. A. Alonso, M. R. Dennis, A. Dudley, A. Forbes, S. Zahedpour, S. W. Hancock, H. M. Milchberg *et al.*, Roadmap on structured waves, *J. Opt.* **25**, 103001 (2023).
- [2] J. B. Pendry, Radiative exchange of heat between nanostructures, *J. Phys.: Condens. Matter* **11**, 6621 (1999).
- [3] K. Joulain, J.-P. Mulet, F. Marquier, R. Carminati, and J.-J. Greffet, Surface electromagnetic waves thermally excited: Radiative heat transfer, coherence properties and Casimir forces revisited in the near field, *Surf. Sci. Rep.* **57**, 59 (2005).
- [4] A. I. Volokitin and B. N. J. Persson, Near-field radiative heat transfer and noncontact friction, *Rev. Mod. Phys.* **79**, 1291 (2007).
- [5] P. Ben-Abdallah and K. Joulain, Fundamental limits for non-contact transfers between two bodies, *Phys. Rev. B* **82**, 121419(R) (2010).
- [6] S.-A. Biehs, M. Tschikin, and P. Ben-Abdallah, Hyperbolic metamaterials as an analog of a blackbody in the near field, *Phys. Rev. Lett.* **109**, 104301 (2012).
- [7] O. D. Miller, S. G. Johnson, and A. W. Rodriguez, Shape-independent limits to near-field radiative heat transfer, *Phys. Rev. Lett.* **115**, 204302 (2015).
- [8] K. Kim, B. Song, V. Fernández-Hurtado, W. Lee, W. Jeong, L. Cui, D. Thompson, J. Feist, M. T. H. Reid, F. J. García-Vidal *et al.*, Radiative heat transfer in the extreme near field, *Nature (London)* **528**, 387 (2015).
- [9] Y. Xiao, M. Sheldon, and M. A. Kats, Super-Planckian emission cannot really be ‘thermal’, *Nat. Photon.* **16**, 397 (2022).
- [10] E. Betzig and J. K. Trautman, Near-field optics: Microscopy, spectroscopy, and surface modification beyond the diffraction limit, *Science* **257**, 189 (1992).
- [11] J. B. Pendry, Negative refraction makes a perfect lens, *Phys. Rev. Lett.* **85**, 3966 (2000).
- [12] X. Wang, A. Díaz-Rubio, V. S. Asadchy, G. Ptitsyn, A. A. Generalov, J. Ala-Laurinaho, and S. A. Tretyakov, Extreme asymmetry in metasurfaces via evanescent fields engineering: Angular-asymmetric absorption, *Phys. Rev. Lett.* **121**, 256802 (2018).
- [13] X. Wang, A. Díaz-Rubio, H. Li, S. A. Tretyakov, and A. Alù, Theory and design of multifunctional space-time metasurfaces, *Phys. Rev. Appl.* **13**, 044040 (2020).
- [14] S. Perea-Puente and F. J. Rodríguez-Fortuño, Complex refraction metasurfaces for locally enhanced propagation through opaque media, [arXiv:2307.03654](https://arxiv.org/abs/2307.03654).
- [15] A. Figotin and I. Vitebskiy, Slow wave phenomena in photonic crystals, *Laser Photon. Rev.* **5**, 201 (2011).
- [16] A. Figotin and I. Vitebskiy, Slow light in photonic crystals, *Waves Random Complex Media* **16**, 293 (2006).
- [17] H. Ramezani, S. Kalish, I. Vitebskiy, and T. Kottos, Unidirectional lasing emerging from frozen light in nonreciprocal cavities, *Phys. Rev. Lett.* **112**, 043904 (2014).
- [18] H. Li, I. Vitebskiy, and T. Kottos, Frozen mode regime in finite periodic structures, *Phys. Rev. B* **96**, 180301(R) (2017).
- [19] M. Y. Nada, T. Mealy, and F. Capolino, Frozen mode in three-way periodic microstrip coupled waveguide, *IEEE Microw. Wireless Compon. Lett.* **31**, 229 (2021).
- [20] H. Li, A. Mekawy, and A. Alù, Gain-free parity-time symmetry for evanescent fields, *Phys. Rev. Lett.* **127**, 014301 (2021).
- [21] L. Ge, Y. D. Chong, and A. D. Stone, Conservation relations and anisotropic transmission resonances in one-dimensional PT-symmetric photonic heterostructures, *Phys. Rev. A* **85**, 023802 (2012).
- [22] R. El-Ganainy, K. G. Makris, M. Khajavikhan, Z. H. Musslimani, S. Rotter, and D. N. Christodoulides, Non-Hermitian physics and PT symmetry, *Nat. Phys.* **14**, 11 (2018).
- [23] L. Feng, R. El-Ganainy, and L. Ge, Non-Hermitian photonics based on parity-time symmetry, *Nat. Photon.* **11**, 752 (2017).
- [24] M.-A. Miri and A. Alù, Exceptional points in optics and photonics, *Science* **363**, eaar7709 (2019).
- [25] S. K. Özdemir, S. Rotter, F. Nori, and L. Yang, Parity-time symmetry and exceptional points in photonics, *Nat. Mater.* **18**, 783 (2019).
- [26] D. Christodoulides and J. Yang, *Parity-Time Symmetry and Its Applications* (Springer, Berlin, 2018).
- [27] K. G. Makris, Z. H. Musslimani, D. N. Christodoulides, and S. Rotter, Constant-intensity waves and their modulation instability in non-Hermitian potentials, *Nat. Commun.* **6**, 7257 (2015).
- [28] I. Krešić, K. G. Makris, U. Leonhardt, and S. Rotter, Transforming space with non-Hermitian dielectrics, *Phys. Rev. Lett.* **128**, 183901 (2022).
- [29] A. Mostafazadeh, Spectral singularities of complex scattering potentials and infinite reflection and transmission coefficients at real energies, *Phys. Rev. Lett.* **102**, 220402 (2009).
- [30] A. Mostafazadeh, Optical spectral singularities as threshold resonances, *Phys. Rev. A* **83**, 045801 (2011).
- [31] S. Longhi, PT-symmetric laser absorber, *Phys. Rev. A* **82**, 031801(R) (2010).
- [32] Y. D. Chong, L. Ge, and A. D. Stone, PT-symmetry breaking and laser-absorber modes in optical scattering systems, *Phys. Rev. Lett.* **106**, 093902 (2011).
- [33] H. Ramezani, H. K. Li, Y. Wang, and X. Zhang, Unidirectional spectral singularities, *Phys. Rev. Lett.* **113**, 263905 (2014).
- [34] A. Mostafazadeh, Nonlinear spectral singularities for confined nonlinearities, *Phys. Rev. Lett.* **110**, 260402 (2013).
- [35] S. Longhi, Spectral singularities and Bragg scattering in complex crystals, *Phys. Rev. A* **81**, 022102 (2010).
- [36] L. Jin and Z. Song, Incident direction independent wave propagation and unidirectional lasing, *Phys. Rev. Lett.* **121**, 073901 (2018).
- [37] V. V. Konotop, E. Lakshtanov, and B. Vainberg, Designing lasing and perfectly absorbing potentials, *Phys. Rev. A* **99**, 043838 (2019).
- [38] H. Moccia, G. Castaldi, A. Alù, and V. Galdi, Harnessing spectral singularities in non-Hermitian cylindrical structures, *IEEE Trans. Antennas Propag.* **68**, 1704 (2020).
- [39] H. Ramezani, Spectral singularities with directional sensitivity, *Phys. Rev. A* **103**, 043516 (2021).
- [40] F. Loran and A. Mostafazadeh, Fundamental transfer matrix for electromagnetic waves, scattering by a planar collection of point scatterers, and anti-PT-symmetry, *Phys. Rev. A* **107**, 012203 (2023).
- [41] A. Yariv, Y. Xu, R. K. Lee, and A. Scherer, Coupled-resonator optical waveguide: A proposal and analysis, *Opt. Lett.* **24**, 711 (1999).
- [42] Here, CROW bands formed by the coupling of other modes in the individual resonators in the CROW are neglected.
- [43] L. E. R. Petersson and G. S. Smith, Role of evanescent waves in power calculations for counterpropagating beams, *J. Opt. Soc. Am. A* **20**, 2378 (2003).

- [44] See Supplemental Material at <http://link.aps.org/supplemental/10.1103/PhysRevB.109.L041405> for details of derivations and circuit simulations. It also contains Refs. [45,46].
- [45] W. E. Lamb and R. C. Retherford, Fine structure of the hydrogen atom by a microwave method, *Phys. Rev.* **72**, 241 (1947).
- [46] E. M. Purcell, Spontaneous emission probabilities at radio frequencies, *Phys. Rev.* **69**, 681 (1946).
- [47] M. F. Limonov, M. V. Rybin, A. N. Poddubny, and Y. S. Kivshar, Fano resonances in photonics, *Nat. Photon.* **11**, 543 (2017).
- [48] P. Peng, W. Cao, C. Shen, W. Qu, J. Wen, L. Jiang, and Y. Xiao, Anti-parity–time symmetry with flying atoms, *Nat. Phys.* **12**, 1139 (2016).
- [49] R. Carminati, J. J. Sáenz, J.-J. Greffet, and M. Nieto-Vesperinas, Reciprocity, unitarity, and time-reversal symmetry of the S matrix of fields containing evanescent components, *Phys. Rev. A* **62**, 012712 (2000).
- [50] H. Li, A. Mekawy, A. Krasnok, and A. Alù, Virtual parity-time symmetry, *Phys. Rev. Lett.* **124**, 193901 (2020).
- [51] R. Carminati, M. Nieto-Vesperinas, and J.-J. Greffet, Reciprocity of evanescent electromagnetic wave, *J. Opt. Soc. Am. A* **15**, 706 (1998).
- [52] C. J. Cattena, L. J. Fernández-Alcázar, R. A. Bustos-Marín, D. Nozaki, and H. M. Pastawski, Generalized multi-terminal decoherent transport: Recursive algorithms and applications to SASER and giant magnetoresistance, *J. Phys.: Condens. Matter* **26**, 345304 (2014).
- [53] E. Domany, S. Alexander, D. Bensimon, and L. P. Kadanoff, Solutions to the Schrödinger equation on some fractal lattices, *Phys. Rev. B* **28**, 3110 (1983).
- [54] PT symmetry for propagating waves in an arbitrary optical system also cannot be maintained when sweeping continuously over frequency due to causality constraints [55].
- [55] A. A. Zyablovsky, A. P. Vinogradov, A. A. Pukhov, A. V. Dorofeenko, and A. A. Lisyansky, PT -symmetry in optics, *Phys. Usp.* **57**, 1063 (2014).
- [56] M. Benzaouia, A. D. Stone, and S. G. Johnson, Nonlinear exceptional-point lasing with *ab initio* Maxwell-Bloch theory, *APL Photon.* **7**, 121303 (2022).
- [57] K. Ji, Q. Zhong, L. Ge, G. Beaudoin, I. Sagnes, F. Raineri, R. El-Ganainy, and A. M. Yacomotti, Tracking exceptional points above the lasing threshold, *Nat. Commun.* **14**, 8304 (2023).
- [58] A. Krasnok, D. Baranov, H. Li, M.-A. Miri, F. Monticone, and A. Alù, Anomalies in light scattering, *Adv. Opt. Photonics* **11**, 892 (2019).
- [59] D. V. Nesterenko, S. Hayashi, and Z. Sekkat, Asymmetric surface plasmon resonances revisited at Fano resonances, *Phys. Rev. B* **97**, 235437 (2018).
- [60] D. V. Nesterenko, S. Hayashi, and V. Soifer, *Ab initio* spatial coupled-mode theory of Fano resonances in optical responses of multilayer interference resonators, *Phys. Rev. A* **106**, 023507 (2022).
- [61] N. Engheta and R. Ziolkowski, *Metamaterials: Physics and Engineering Explorations* (Wiley, New York, 2006).
- [62] A. Alù and N. Engheta, Pairing an epsilon-negative slab with a mu-negative slab: Resonance, tunneling and transparency, *IEEE Trans. Antennas Propag.* **51**, 2558 (2003).
- [63] A. Alù and N. Engheta, Physical insight into the “growing” evanescent fields of double-negative metamaterial lenses using their circuit equivalence, *IEEE Trans. Antennas Propag.* **54**, 268 (2006).
- [64] Z. Chen, Z. Li, J. Weng, B. Liang, Y. Lu, J. Cheng, and A. Alù, Sound non-reciprocity based on synthetic magnetism, *Sci. Bull.* **68**, 2164 (2023).